An Experimental Characterisation of the Wake of a Detailed Heavy Vehicle in Cross-Wind.

Damien McArthur, David Burton, Mark Thompson and John Sheridan

Department of Mechanical and Aerospace Engineering, Monash University, Clayton 3800, Australia

Abstract

The unsteady wakes associated with detailed heavy vehicles with different levels of passive aerodynamic treatment are investigated in a wind tunnel using a 1/3 scale model. Drag coefficient, base pressure and wake total pressure are measured for detailed vehicles at yaw angles up to 15° for six semi-trailer vehicle configurations. Cabin extenders and side-skirts were shown to be more effective at reducing drag under yawed flow conditions, while certain front-end modifications were found to perform best at $\psi = 0°$ when the tractor was more able to shield the trailer from oncoming flow.

Base pressure was shown to reduce with yaw angle, with the low pressure signature of the main lower vortex tilting upwards on the leeward side of the vehicle's base. Total pressure grid measurements showed two different types of wake, those where the stream-wise vortex formed by flow separating off the roof of the trailer is separated from the bulk vehicle wake by a region of high total pressure, and those where the two are indistinguishable. Vehicles without a distinct trailing vortex in this region were found to exhibit stronger horizontal asymmetries in their base pressure profiles.

Keywords:

Bluff Body, Wake, Heavy Vehicle, Aerodynamics, Square Back, Truck, Yaw, Cross-wind

1. Introduction

Flows over heavy vehicles in cross-winds are important for a number of reasons. Whilst aerodynamic drag is perhaps the most studied because of its direct links to fuel economy and transports costs, cross-wind flows alter vehicle stability, cornering, water / mud spray and wind noise (Weir 1980; Garry and Cooper 1986; Hucho 1987; Cheli et al. 2006; Gaylard and Duncan 2011). Heavy vehicles can be particularly sensitive to the effects of cross-wind. Having a significantly greater length than width can lead to large side forces, while the sharp edges on the upper sides of the trailer promote separation and the generation of stream-wise vortices, which in turn affect vehicle aerodynamic drag.

The yaw angle (ψ) seen by a vehicle is a function of vehicle speed, wind speed and wind incidence angle. It is suggested in Hucho (1987) that the range of yaw angles needing to be considered is in the region of $\psi = \pm 14°$ based on stationary measurements of wind data as well as the work of Gardell (1980), who based calculations on a vehicle speed of 80 km/h with an 18 km/h crosswind. Scaling this to typical Australian speed limits of 100 km/h reduces the effective yaw range to $\psi = \pm 10°$.

There have been many studies showing the benefits of additional add-on devices, such as side-extenders, boat-tails, and side skirts in lowering aerodynamic drag (Cooper and Leuschen 2005; Leuschen and Cooper 2006; Burton et al. 2011; Cooper 2012; Burton et al. 2013), the latter of which considers the configurations studied herein. It is common practice in wind tunnel testing of a heavy vehicle or add-on device to present forces and moments over a range of yaw angles e.g. (Storms et al. 2004; Cooper and Leuschen 2005; Landman et al. 2010). Additionally SAE (2012) defines a wind-averaged drag coefficient, which is a weighted average of drag across the set of expected ambient conditions.

Croll et al. (1996) shows that the far wake of the Ground Transportation System (GTS), a simplified heavy vehicle with rounded forebody corners and length to width ratio similar to heavy vehicles, at $\psi = 10°$ is dominated by a pair of stream-wise, counter-rotating vortices. A number of computational investigations have attempted to match the GTS flow-field at $\psi = 10°$. While none manage to capture the correct near wake (the region of the wake prior to the closure of the dividing streamlines), simulations do show that the stream-wise vortices noted above originate from separation over the upper stream-wise edges of the vehicle (Salari et al. 2004; Maddox et al. 2004).

Van Raemdonck (2012) presented mean base pressure and a PIV velocity field in the half height plane for the simplified GTS model at a yaw angle of 6°. On the leeward side of the vehicle's base, pressure is reduced relative to the 0° baseline. The velocity field shows that the leeward side, time averaged vortex is enlarged, while the rear stagnation point is shifted towards the windward side of the base. Comparable numerical results show that the RANS simulation employed is unable to replicate this horizontally asymmetric recirculating wake.

Storms et al. (2006) showed base pressure contours as well as tractor-trailer gap PIV for the GCM model at $\psi = 10°$. CFD by Hyams et al. (2011) shows unsteady structures exiting the tractor-trailer gap on the leeward side and convecting downstream towards the wake. Heineck et al. (2004) showed that a dramatic reduction in drag, measured between $\psi = 10°$ and $\psi = 11°$ is related to the core of the main gap vortex moving from the windward to the leeward side, which was accompanied by a significant reduction in both vertical flow and flow through the gap.

When the oncoming flow is angled relative to the vehicle's longitudinal axis, a number of different flow structures will develop. Figure 1 shows a pair of co-rotating stream-wise vortices separating from the roof trailer. This system is equivalent to that seen on a finite aspect ratio wing with endplates. Due to under-body blockage, the flow field beneath the trailer will be more complex.

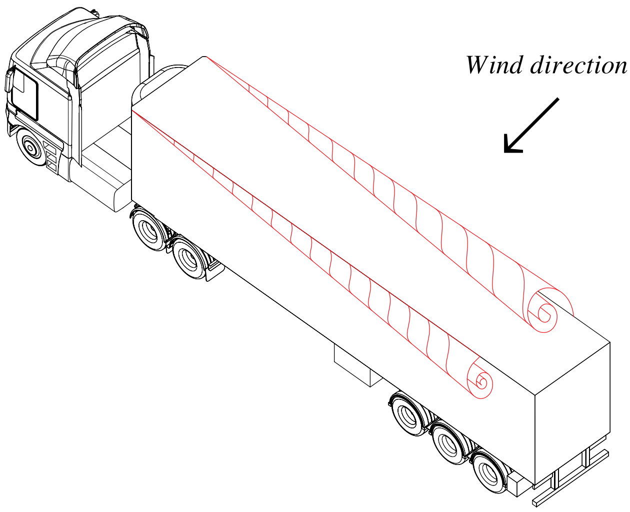

Figure 1: Development of stream-wise vortices along a heavy vehicle in cross-wind.

Despite the body of knowledge presented above, there still remain questions about the influence of cross-winds on heavy vehicles, particularly relating to the change in aerodynamic response between simplified and detailed vehicles. Wind incidence angle is known to have a non-linear effect on drag as well as other aerodynamic forces and moments. In fact, the effectiveness of individual add-on components may not even be directionally consistent, with some devices providing maximum drag reduction at 0° yaw, while others perform better with increasing wind incidence.

Many wind tunnel and CFD investigations present curves of drag versus yaw angle, both for entire vehicles and as individual component deltas, however considerably less information is available regarding the flow-fields associated with detailed vehicles at yaw. A recent study in a water channel (McArthur et al. (2016)) has provided detailed information into the time varying wake behind simplified and detailed heavy vehicles, however, cross-wind effects were not considered.

Unlike some other ground transport modes, such as high speed trains, a wide variety of heavy vehicle configurations continue to be adopted, primarily because of the large number of often competing requirements, in addition to aerodynamics, that heavy vehicles must fulfil. The aerodynamic challenge faced by the industry is not always one that allows the adoption of a highly streamlined body, rather it is a need to balance requirements including length limits, manoeuvrability, robustness, cost, etc. with aerodynamic performance.

To this end this paper aims to elucidate the effects of cross wind on a number of detailed heavy vehicle configurations by presenting base pressure and wake total pressure measurements behind a 1 : 3 scale heavy vehicle model.

2. Methodology

2.1. Experimental facility

Testing was carried out in the Monash University 1.4MW wind tunnel. In order to account for the large blockage, a number of modifications were made to the $\frac{3}{4}$ open jet test section. Details of the modifications and results of the subsequent flow validation are presented in McArthur et al. (2013). The velocity profile and distribution were obtained using a four-hole dynamic pressure probe that was traversed in the empty tunnel at a point 3.75 metres upstream of the turntable centre, approximately equivalent to the location of the leading edge of the model. The coefficient of variation in mean velocity was ¡ +/- 0.75% over the area of the model. The displacement thickness increases from 10mm at the start of test section to 25mm at four metres downstream from the centre of the turntable, at the front of the model it is 12mm, which is 14% of the frontal ground clearance. The mean streamwise turbulence intensity outside of the boundary layer is 1.6%.

The final solid blockage ratio was 10.6%, flow mapping was conducted at a width based Reynolds number ($Re_W = \frac{U_0 \times W}{\mu}$) of 1.4×10^6, corresponding to the maximum rated velocity of the wind tunnel traverse system. Measurements presented in McArthur et al. (2013) show that the vehicle's drag coefficient has not become independent of Reynolds number, although the variation with increasing velocity is small and consistent, hence it is expected that measurements at this reduced Reynolds number can provide relevant insight into the wakes of vehicles at operational speeds. The origin of the wind tunnel coordinate system for this investigation is the centre of the lower edge of the base of the vehicle. The X-axis is in the downstream direction, the Z-axis is vertically upwards and the Y-axis follows from a conventional orthogonal coordinate system.

2.2. Model geometry

The geometry used for this investigation is a 1:3 scale model of a commercially available Cab-over-Engine (CoE) tractor mated to a commercially available articulated box-trailer. The overall model dimensions are height H = 1,400mm, width W = 830mm, length L = 6,000mm, tractor-trailer gap G = 680mm and ground clearance at the front of the truck = 83mm. Key dimensions are shown in Figure 2. Details of the model and results of a comprehensive drag reduction program have been published in Burton et al. (2013). In this investigation a number of configurations of the CoE model are selected for flow mapping, this is intended to allow characterisation of a range of heavy vehicle wakes, representative of different vehicles currently in operation. For example, by testing with a relative large gap, then adding side extenders and finally closing the gap in full a wide range of gap flows is studied. Similarly, the progressive addition of side skirts and boat tails enables a low drag, streamlined configuration to be achieved.

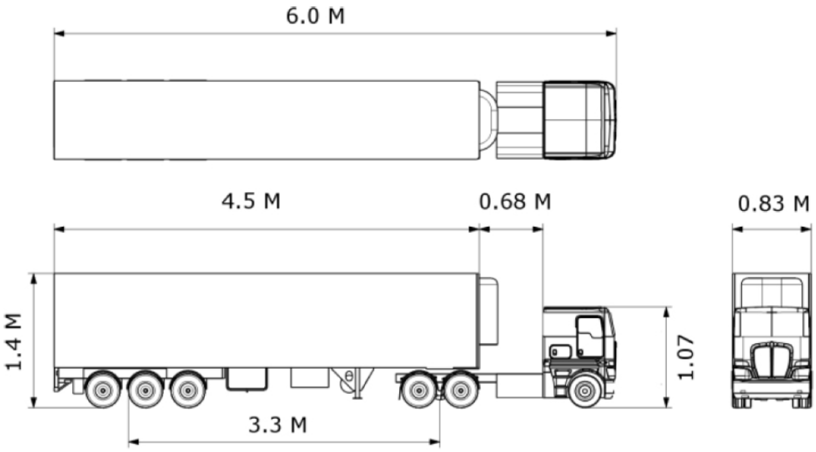

Figure 2: Scale model key dimensions.

Figure 3 shows the model installed in the wind tunnel in both high drag and low drag configurations.

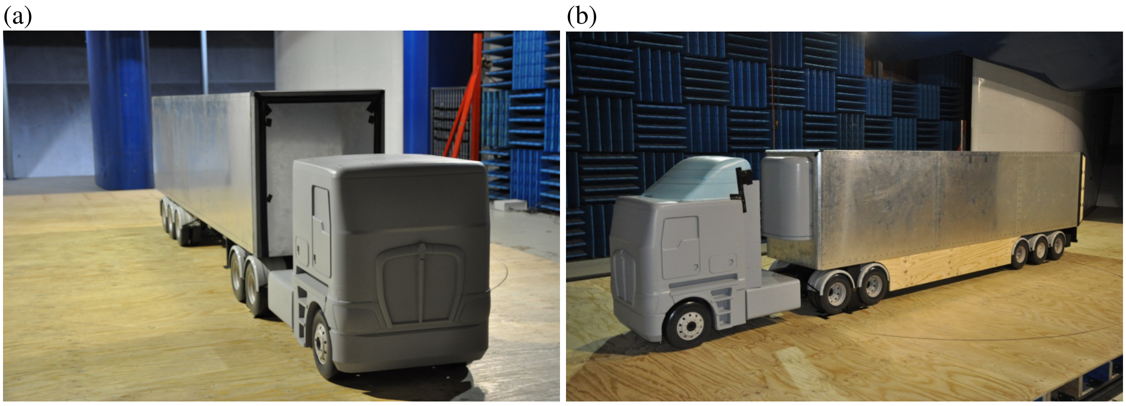

Figure 3: Detailed 1 : 3 scaled model. (a) high-drag baseline, (b) low-drag configuration.

To further understand the wakes of different heavy vehicles a number of typical configurations were defined. The geometries of interest are detailed below in order of decreasing drag coefficient see Figure 4(a).

The *Sharp* vehicle is the highest drag model tested and consists of flat top cab in front of a trailer with sharp leading edges. The *Flat* vehicle also employs the flat top cab. In this configuration the trailer is equipped with rounded leading edges and an external refrigeration unit. The *Fairing* vehicle incorporates a sleeper cab tractor with a roof fairing and angled side extenders that are $0.165G$ long and angled outwards at 15deg. Once again the trailer is equipped with rounded leading edges and an external refrigeration unit. The *Closed* vehicle includes the fairing cab, $1.0G$ long side extenders and an additional surface that is sealed from the trailing edge of the roof fairing to the leading edge of the trailer, thus eliminating the tractor-trailer gap. The *Closed-Skirts* model is the same as the Closed, with the addition of trailer-mounted side-skirts that cover 79% of the trailer ground clearance height. The *Boat-tail* model is the same as the Closed-Skirts, with the addition of $0.24W$ long boat-tails, placed on the upper and side trailing edges of the vehicle at an

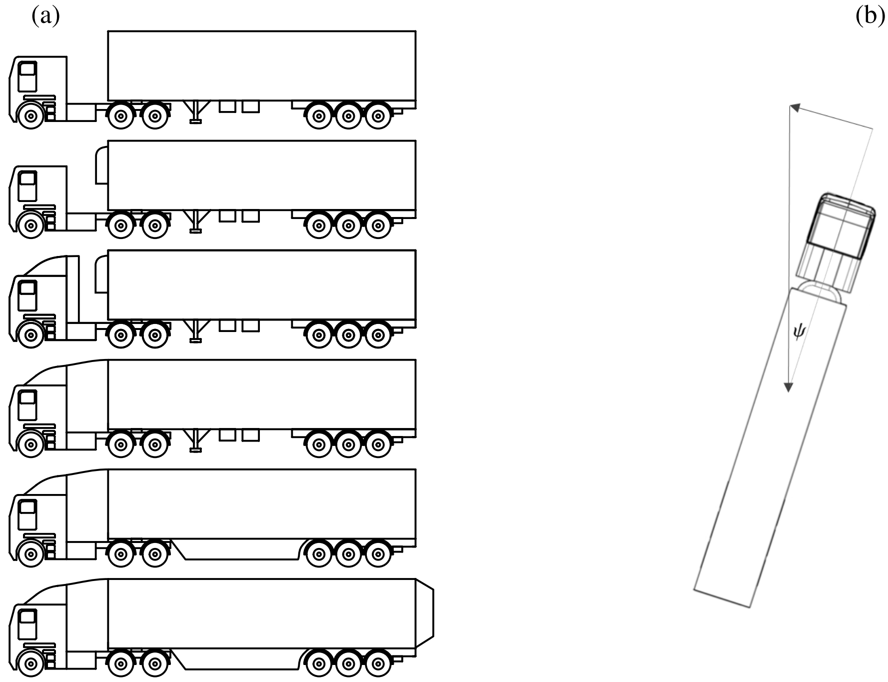

Figure 4: (a) Schematics of model configurations, from top to bottom in order of decreasing drag coefficient: Sharp, Flat, Fairing, Closed, Closed Skirts, Boat-tail. (b) Yaw angle (ψ) shown as the angle (positive here) between the vehicle direction of travel and the resultant wind direction.

angle of 15°.

The four main front-end configurations chosen reflect not only variations among the range of drag values seen in typical heavy vehicles, but, in addition, each has a fundamentally different interaction between the cabin and trailer, which has an influence on the development of the flow-field downstream of this region. In the Closed configuration, the cab and trailer are effectively a single body. In this situation the flow stagnates at the front of the vehicle and then the boundary layer develops continuously down the upper and side faces of the truck/trailer.

The Fairing cab is the first of the two-body systems, where flow separates from the tractor and reattaches on the trailer. In this configuration the roof fairing and side extenders serve to shield the trailer from incoming flow so there is not a significant stagnation of flow on the front face of the trailer and the separating shear layer from the cabin joins with the boundary layer along the top and sides of the trailer.

The Flat cab does without either the roof fairing or side extenders. This means less flow is deflected away from the trailer and consequently, more high speed flow interacts with the front face of the trailer. As the front of the trailer has a curved refrigeration unit and rounded leading edges, the boundary layer that begins on the front of the trailer remains attached along these convex surfaces.

The Sharp configuration represents the final category of tandem body aerodynamics, where flow once again interacts with the front face of the trailer, but due to the sharp leading edges, undergoes large-scale separation.

2.3. Measurement equipment

Force measurements are obtained using an underfloor balance consisting of 4 by 3-component Kistler force piezoelectric transducers connected through a floating frame, see Tropea et al. (2007) for the application of this technique. The model is connected to the underfloor force balance via 4 support posts, 2 running down through the centre of the front wheel bogey and 2 through the rear wheel bogey. The coefficient of variation of the force measurements is +/-0.5%.

Pressure measurements were taken using a Dynamic Pressure Measurement System (DPMS). The DPMS has 64 available channels, all connected to a common reference which was plumbed to a plenum outside the flow of the test section. Two DPMS units were used, one with full scale measurement range of ±3.0 kPa and one with ±7.0 kPa. The manufacturer claimed accuracy of these units is ±0.1% of full scale output. The system was calibrated in house by connecting to a Betz manometer.

The DPMS is capable of sampling at frequencies up to 1,000 Hz, but in practice the maximum frequency that can be resolved is limited by damping in the tube system connecting the DPMS to the measurement location. In order to account for distortion to the time varying pressure signal, an inverse transfer function correction is used. For the set-ups detailed below this allowed accurate determination of frequencies up to the Nyquist frequency of 500Hz ($St_W = 14.8$)

Surface pressure measurements were taken on the rear face of the model by connecting 500mm long ⌀1.2mm PVC tubes to the DPMS. The taps were arranged in a 7×7 array with span-wise and vertical spacings of $0.16W$ and $0.17W$ respectively (figure 5a). Measurements were taken for 60 seconds at a sampling rate of 1,000 Hz.

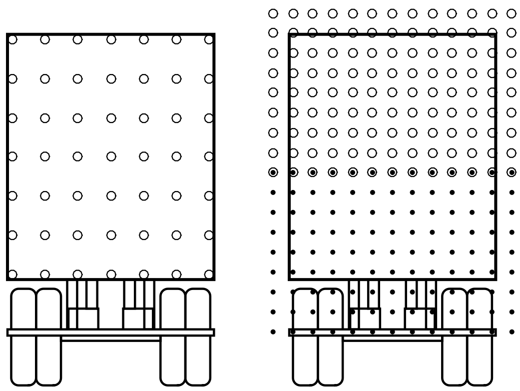

Figure 5: Schematic of base pressure tap and total pressure grid locations. Probe locations for the upper (○) and lower (●) total pressure grids.

In order to obtain simultaneous data across a large spatial region in the wake, a 13×9 rectangular grid of forward facing tubes was used with spacing equal to $0.096W$. The quantity measured by this device is the stream-wise component of total pressure ($p + 1/2\rho u^2$). As these tubes are forward facing, they can only obtain reliable data for flow incidence angles within a cone of acceptance before separation effects begin to dominate. Bell (2015) yawed a grid of total pressure probes through -20° to 45°, finding that for incidence angle magnitudes up to 16° the measured velocity agreed with the true velocity component. Beyond ±16° the probe measurements dropped off more quickly than the true component of dynamic pressure. The grid was placed at two heights (Z=225mm to 855mm and Z=855mm to 1495mm) to capture the upper and lower regions of the wake. Figure 5 shows the total pressure grid measurement locations in relation to the base of the vehicle.The probes were connected to the DPMS via 2200 mm long, ⌀1.5mm PVC tubing, resulting in a maximum resolvable frequency of 500 Hz. Measurements were taken for 60 seconds at a sampling rate of 1,000 Hz.

In order to assess any blockage effects caused by the total pressure grid, the low grid was placed at various distances downstream of a 1 : 3 scale Ground Transportation System (GTS) model (figure 6a) while measuring both the models drag and base pressure. Figure 6b shows the change in drag and mean base pressure. In all cases the change in drag and base suction are of similar magnitude, suggesting that the blockage effects are largely confined to the rear of the vehicle. At $X = 1W$ the drag and base pressure have similar values to those without the grid, while moving the grid further downstream caused a drag reduction of approximately $\Delta C_D = -0.015$.

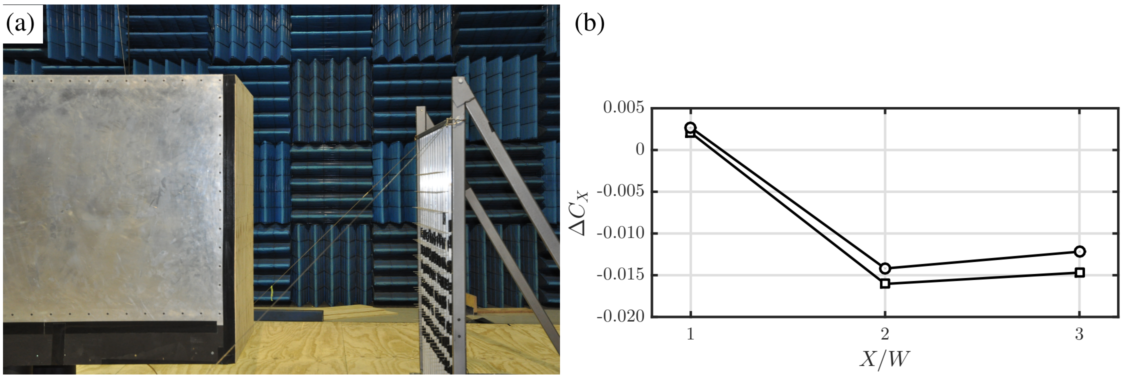

Figure 6: (a) Total pressure grid installed 1W behind a simplified GTS model, (b) Variation of drag (□) and base pressure drag (○) on the GTS with stream-wise position of the lower total pressure grid

Contours of mean base pressure in figure 7, each plotted on its own colour scale, show that with the grid at $X = 1W$, even though the spatially averaged base pressure is close to the baseline value, there are differences in the topology, indicative of some interference effects. For $X = 2W$ & $3W$ however the base pressure contours agree remarkably well with the baseline. This shows that at these distances the influence of the grid is to cause an adverse static pressure gradient, rather than to modify any flow structures.

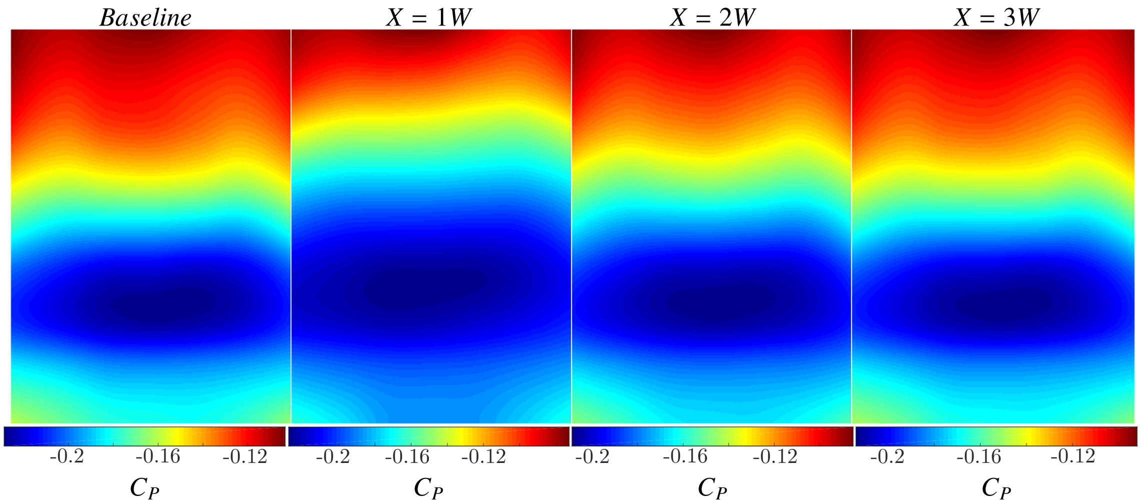

Figure 7: GTS base pressure contours with low total pressure grid installed.

3. Results

Mean base pressure measurements are presented in figure 8a relative to zero degree yaw case for each configuration. These show that the Sharp and Flat configurations had a faster loss of base pressure with yaw compared to the more streamlined vehicles, particularly for yaw angles above 5°. This is in the opposite direction to the trends for drag in figure 8b, presented relative to the drag of the Sharp case at zero degrees yaw. This suggests that increments in drag with yaw occur mainly due to local flows at the front of the vehicle and under-body. The Closed case is of particular interest, the drag coefficient increases rapidly with yaw and is even higher than the Sharp case at 10° yaw, indicating a dominance of the underbody flow, given the effect is removed by the addition of side skirts (Closed Skirts). The Sharp, Flat and Fairing cases, those with an open gap, exhibit relatively flat drag coefficient curves up until 5°, and the small drag increases in this range are attributed, in part, to the reduction in base pressure. In other words, the front-end flow has only a minor effect in this range. It is noted that the dynamic pressure used to determine coefficients herein is the resultant dynamic pressure, which is held constant for all yaw angles, a corollary of this is that the component of the resultant dynamic pressure due to forward speed reduces with increasing yaw.

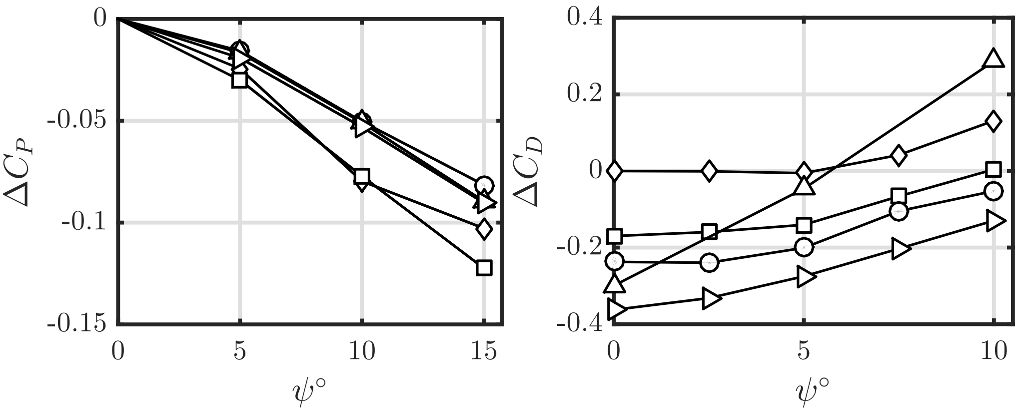

Figure 8: (a) Change in mean base pressure coefficient with yaw angle and (b) Change in drag coefficient with yaw angle: ◇ Sharp, □ Flat, ○ Fairing, △ Closed, ▷ Closed Skirts.

Mean base pressure contours in figure 9 show a progressive strengthening and tilting of the low pressure region associated with the main lower vortex for all configurations. The lower pressure across the upper half of the leeward side of the base, particularly at high yaw angles, suggests that the vertical arm of the time-averaged wake vortex ring is moved further upstream, while the high pressure region on the windward side of the base indicates that the rear stagnation point has moved in that direction. At higher yaw angles the Sharp and Fairing vehicles have the highest levels of horizontal asymmetry in the upper part of the base.

In order to capture the enlarged wake created by yawing the vehicle, the total pressure grid was placed at $X = 1W$ and translated by $0.48W$ in the Y direction. The vehicle was then swept from $\psi = -15°$ to $\psi = 15°$ in increments of 5°. Pressure fields for negative yaw angles were then mirrored and combined with those at positive yaw angles. This was done for both the upper and lower grid positions to create the pressure fields in figure 10.

Two main differences can be seen between the wake of the Closed Skirts and Fairing models as yaw angle increases. Firstly an isolated low total pressure region can be seen on the leeward side of the upper part of the Closed Skirts bulk wake. This is the stream-wise vortex that forms due to roll-up of boundary layer flow separating from the roof of the trailer. The size and pressure deficit of this vortex increase with yaw angle in the same manner as tip vortices on a finite-aspect-ratio wing. For the Fairing case, which allows flow to bleed through the tractor-trailer gap, this structure is much less concentrated and its low total pressure signature extends into the bulk wake.

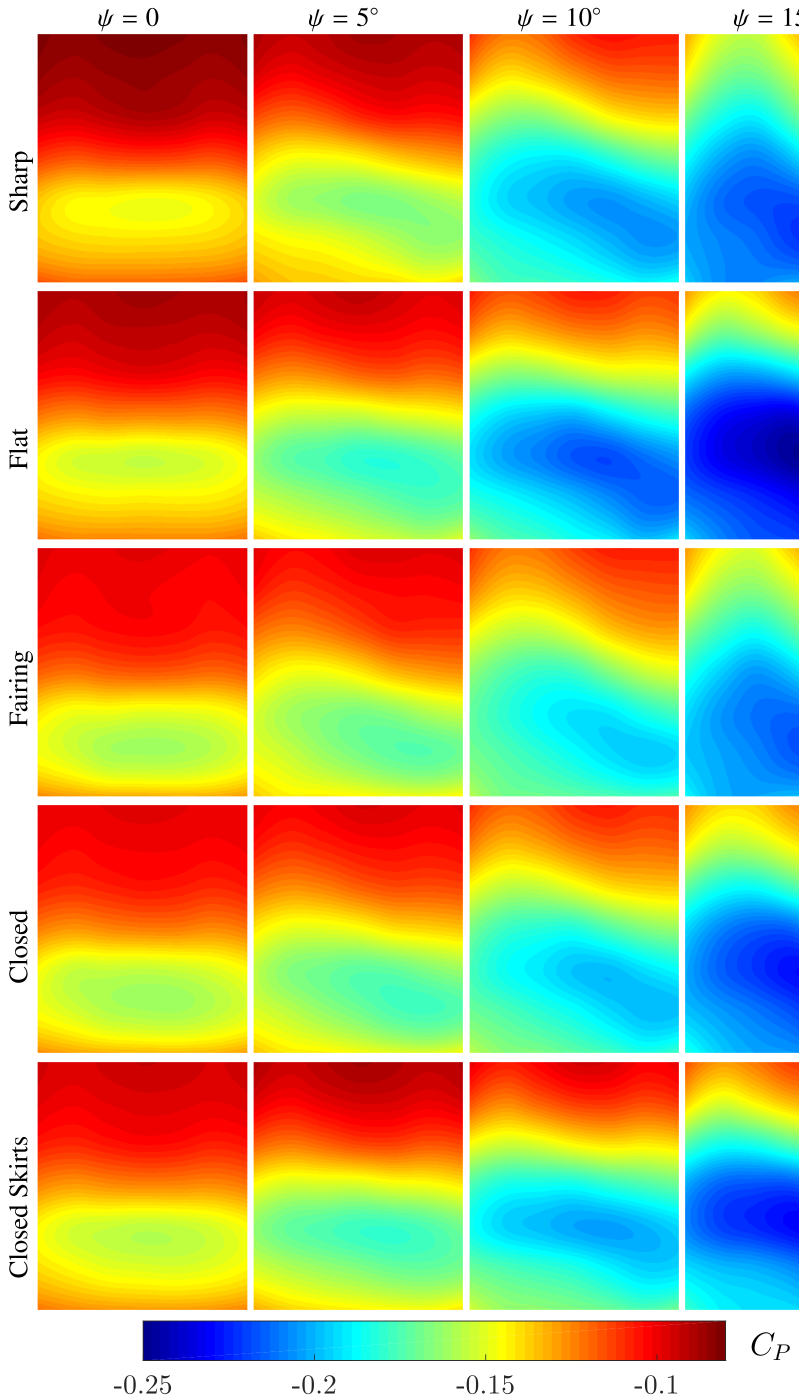

Figure 9: Base pressure variation with vehicle yaw.

The other main difference between the two fields is in the lower wake on the leeward side. Here the fairing configuration shows a much larger region of reduced pressure. This is a result of flow separation off bluff components in the trailer under-body, while the configuration with side-skirts blocks flow from this region and does a better job of maintaining attached flow on the leeward side of the trailer.

Figure 11 shows the central region total pressure at $X = 1W$, $\psi = 15°$ for each configuration. The Closed

Skirts, Closed and Fairing all have discrete stream-wise vortices, while the Fairing and Sharp configurations do not. The reason for this is that the two Closed models have no tractor-trailer gap, allowing continuous development of the rooftop vortex from the start of the vehicle, while for the Flat model at yaw, the cabin is too low to affect flow over the roof. In this configuration airflow stagnates on the front of the trailer and remains attached over the roof before separating from the leeward side of the trailer roof to form the vortex. The other two configurations however, both have separated or turbulent flow on the roof and along the leeward side of the trailer. For the Fairing vehicle, flow through the tractor trailer gap and only partial shielding of the upper region of the trailer cause separation and turbulent structures that convect down the leeward side of the vehicle, as seen in the GCM simulation of Hyams et al. (2011), while for the Sharp configuration flow immediately separates from the sharp edges at the front of the trailer.

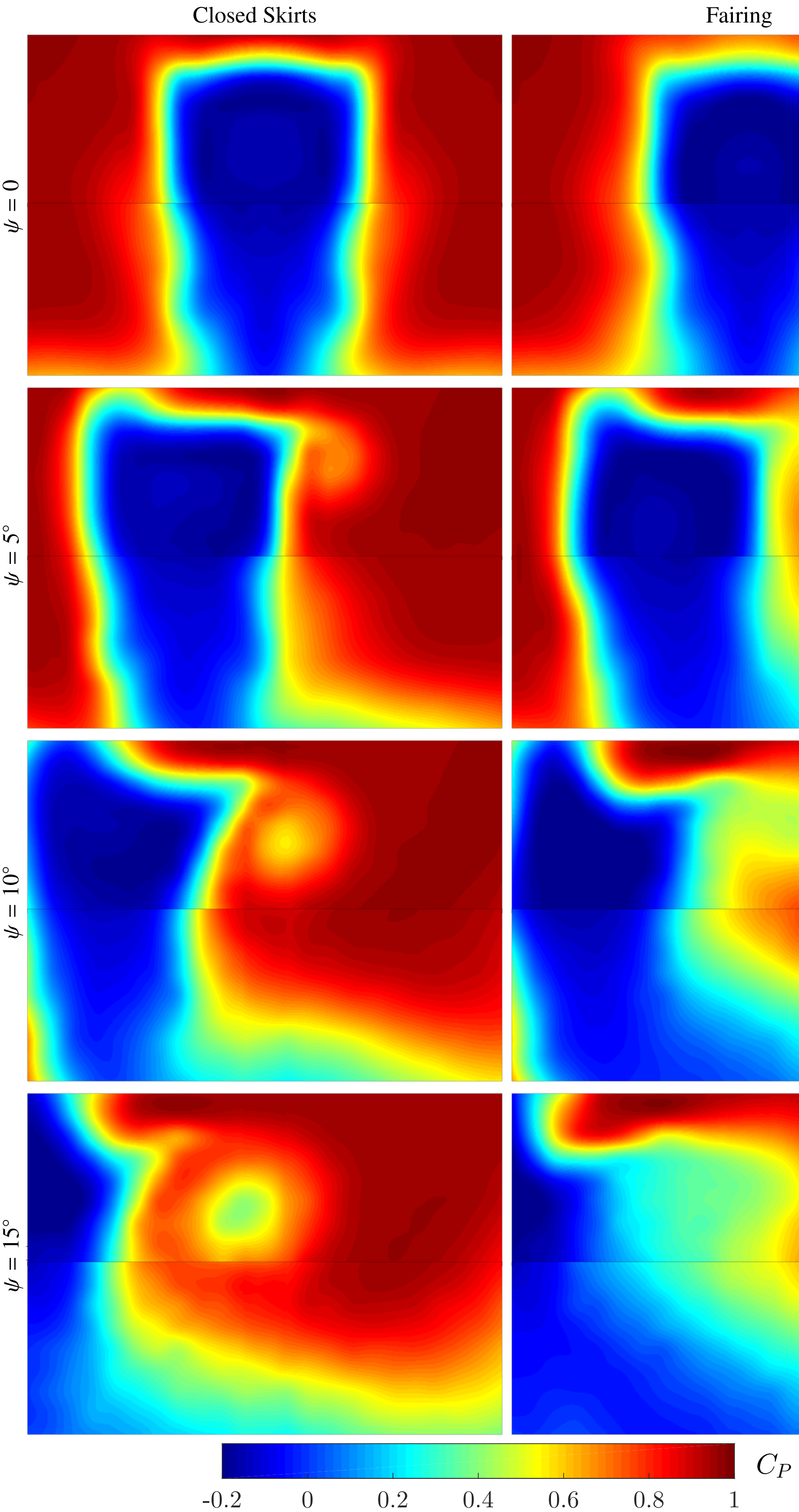

Figure 10: Stream-wise total pressure fields for $X = 1W$, composited from 4 individual measurements. Column 1 Closed Skirts, Column 2 Fairing. Total pressure grids are fixed in tunnel aligned coordinates.

The configurations with isolated vortices (Closed Skirts, Closed and Flat) are also the configurations with more horizontally symmetric base pressure profiles in figure 9, while those without distinct vortices (Fairing and Sharp) have strongly asymmetric base pressure profiles at large yaw angles.

A possible explanation for this is that the presence of the uninterrupted vortex causes an induced velocity which brings high speed flow towards the surface of the trailer, allowing for a more normal boundary layer to develop as opposed to the configurations that are dominated by upstream separation.

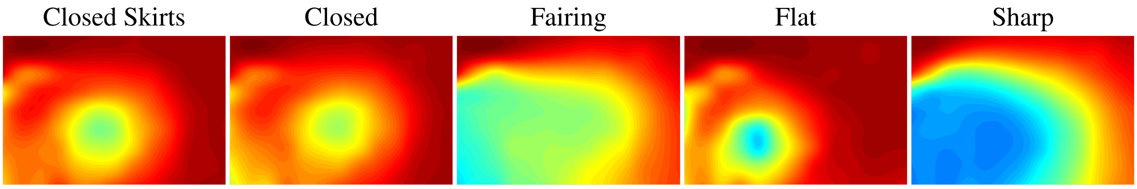

Figure 11: Stream-wise total pressure fields $X = 1W, \psi = 15°$. Total pressure grid is fixed in tunnel aligned coordinates. Colour scale is the same as figure 10.

Total pressure fields for the Closed Skirts vehicle at $X = 1, 2$ & $3W$ (figure 12), show that the trajectory of the tip vortex is both downwards and inwards towards the centre axis of the vehicle. The same trend is observed for other configurations, results of which are presented in the Appendix.

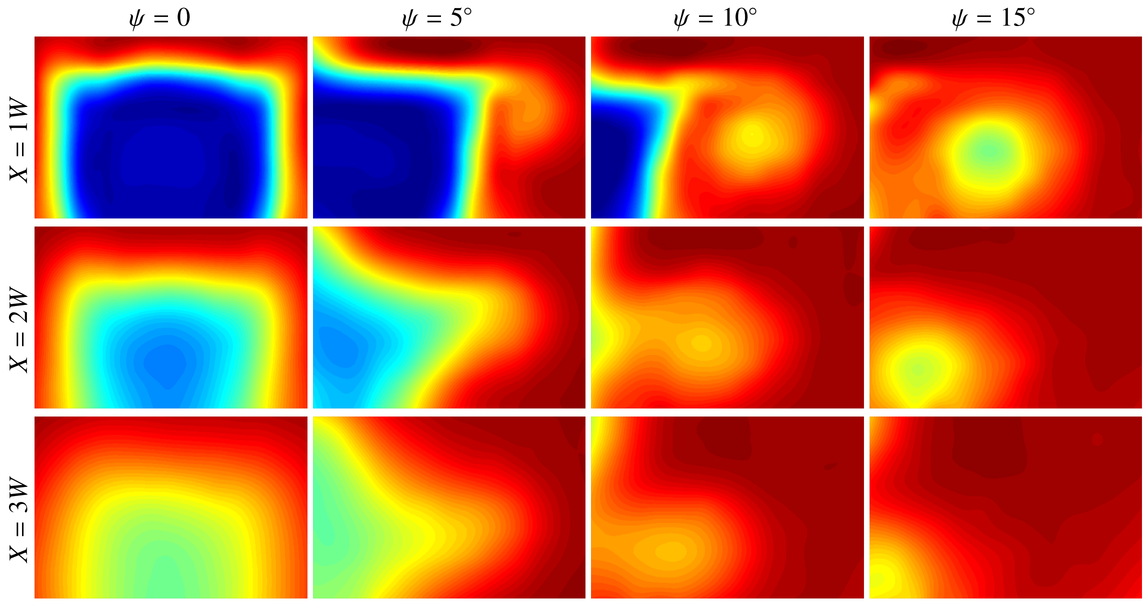

Figure 12: Stream-wise total pressure fields for Closed Skirts vehicle at $X = 1, 2$ & $3W$. Total pressure grid is fixed in tunnel aligned coordinates. Colour scale is the same as figure 10.

3.1. Boat-tails

The largest change in wake flow at $\psi = 0°$ comes from the addition of boat-tails. Figure 13 shows the upper wake total pressure field for the boat-tail vehicle $1W$ behind the base at yaw angles of $\psi = 0°, 5°, 10°\&15°$. At all incidence angles the bulk wake captured within this measurement area is significantly smaller than the corresponding region for the Closed Skirts model (figure 10. The distinct leeward streamwise vortex is once again observed, and there is possible evidence of another vortex above the bulk wake, which forms from the upper windward longitudinal trailer edge.

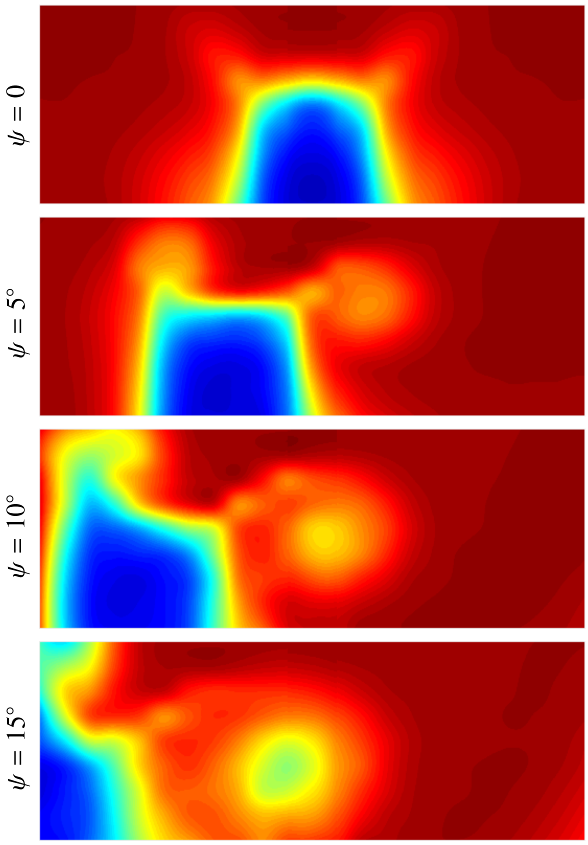

Figure 13: Boat-tail configuration, mean total pressure fields in the upper half of the wake, $X = 1W$. Colour scale is the same as figure 10.

4. Base pressure Proper Orthogonal Decomposition (POD)

Turbulent flows, such as bluff body wakes contain a mix of coherent and chaotic motions that are spread over a range of scales. It can be of great benefit to be able to extract the dominant fluctuating structures from a set of instantaneously measured flow fields. The aim of reduced order modelling is to decompose a set of flow fields into independent modes, the most relevant of which can be combined to reconstruct the flow features of interest, free from the obfuscation of small scale turbulence of other structures of lesser importance. Proper Orthogonal Decomposition (POD) achieves this by extracting the successive spatial modes which minimise the variance of all remaining elements. A review of the derivation and implementation of POD for turbulent flows can be found in Berkooz et al. (1993).

A POD was constructed on the time-resolved base pressure measurements of the Closed vehicle at yaw angles of $\psi = 0,\ 5,\ 10\ \&\ 15°$. Mode rankings in figure 14 show that the fraction of total fluctuating content within modes 1-3 decreases with increasing yaw angle.

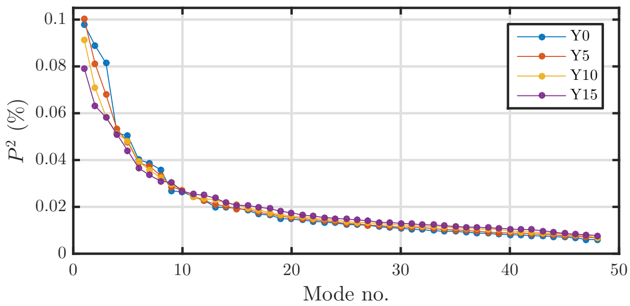

Figure 14: Base pressure POD mode rankings.

In each case, the base pressure POD contains a pair of low frequency modes corresponding to vertical fluctuations and a horizontal mode fluctuating at $St_W \approx 0.2$, suggestive of von Kármán-like shedding.

The structure of Vertical modes 1 & 2 shows a progressive tilting between $\psi = 5°$ and $\psi = 15°$ (figure 15). There are signs of an antisymmetry between the $\psi = 0°$ and $\psi = 5°$ cases, suggesting that some part of the near wake process may be inherently unstable in a fully symmetrical state.

At higher yaw angles the mode spectra of Vertical Mode 1 becomes dominated by a broad peak at $St_W \simeq 0.13$. The von Kármán-like peak in Horizontal Mode 1 is apparent for all cases, but at high yaw angles it is overshadowed by lower frequency content.

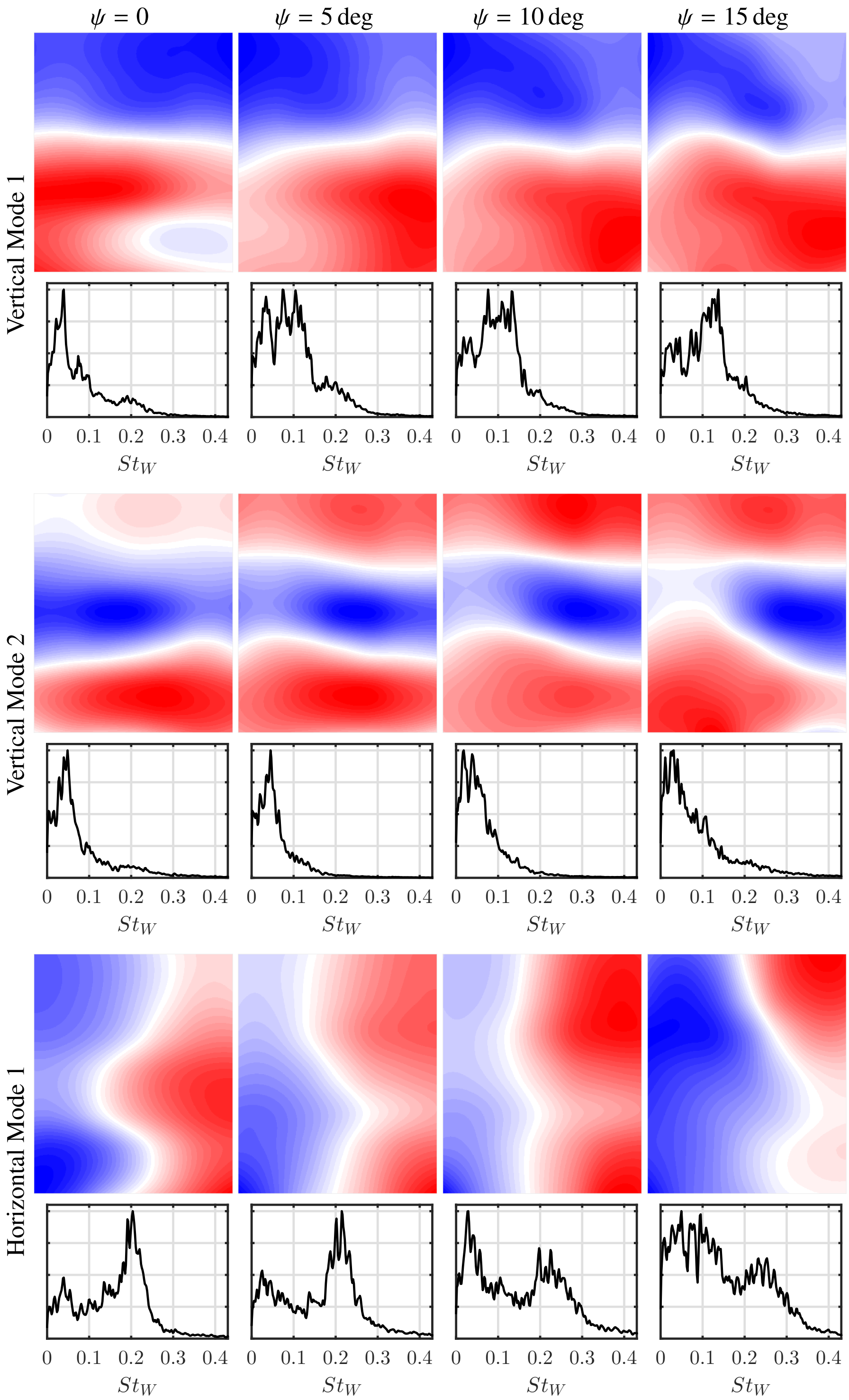

Figure 15: Closed vehicle base pressure POD modes 1-3.

5. Conclusions

This paper has presented drag, base pressure and wake total pressure measurements for detailed vehicles at yaw angles up to 15°. Cabin extenders and side-skirts were shown to be more effective at reducing drag under yawed flow conditions, while certain front-end modifications were found to perform best at $\psi = 0°$ when the tractor was more able to shield the trailer from oncoming flow.

Base pressure was shown to reduce with yaw angle, with the low pressure signature of the main lower vortex tilting upwards on the leeward side of the vehicle's base. Total pressure grid measurements showed two different types of wake, those where the stream-wise vortex formed by flow separating off the roof of the trailer is separated from the bulk vehicle wake by a region of high total pressure, and those where the two are indistinguishable. Vehicles without a distinct trailing vortex in this region were found to exhibit stronger horizontal asymmetries in their base pressure profiles.

6. Additional Figures

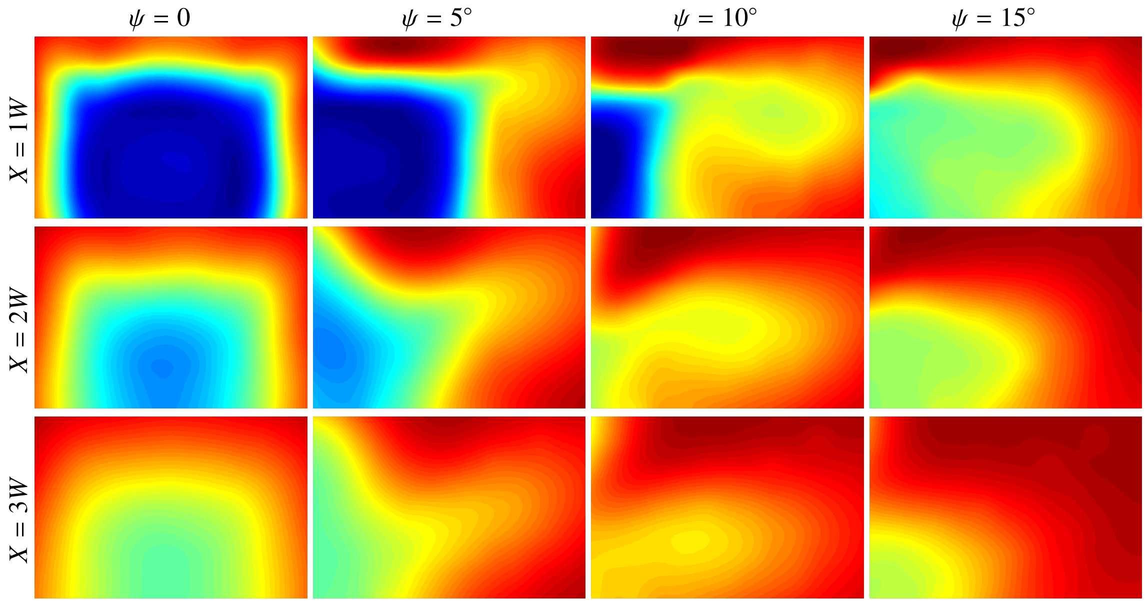

Figure 16: Stream-wise total pressure fields for Fairing vehicle at $X = 1$, 2 & $3W$. Total pressure grid is fixed in tunnel aligned coordinates. Colour scale is the same as figure 10.

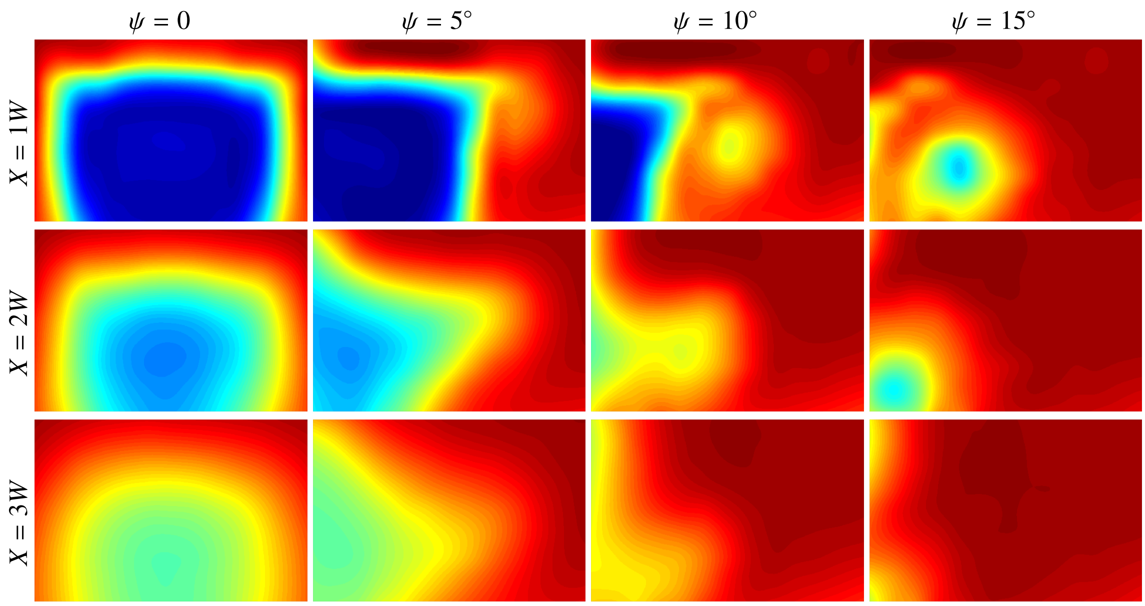

Figure 17: Stream-wise total pressure fields for Flat vehicle at $X = 1,\ 2\ \&\ 3W$. Total pressure grid is fixed in tunnel aligned coordinates. Colour scale is the same as figure 10.

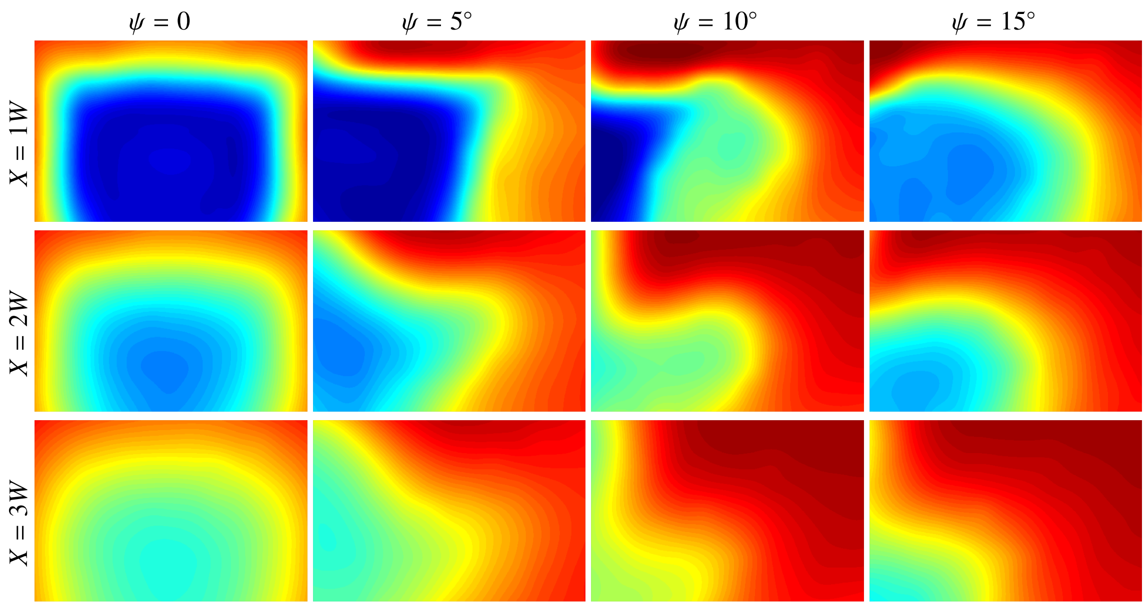

Figure 18: Stream-wise total pressure fields for Sharp vehicle at $X = 1,\ 2\ \&\ 3W$. Total pressure grid is fixed in tunnel aligned coordinates. Colour scale is the same as figure 10.

Acknowledgements

This research was supported under the Australian Research Council's *Linkage Projects* funding scheme (project number LP0991170).

References

Bell, J. R., 11 2015. The slipstream and wake structure of high-speed trains. Ph.D. thesis, Monash University, Melbourne, Australia.

Berkooz, G., Holmes, P., Lumley, J. L., 1993. The proper orthogonal decomposition in the analysis of turbulent flows. Annual review of fluid mechanics 25 (1), 539–575.

Burton, D., McArthur, D., Sheridan, J., Thompson, M., 09 2013. Contribution of add-on components to the aerodynamic drag of a cab-over truck-trailer combination vehicle. SAE Int. J. Commer. Veh. 6, 477–485.
URL http://dx.doi.org/10.4271/2013-01-2428

Burton, D., Nazarinia, M., Sheridan, J., Parkin, D., 2011. Optimisation of boat-tails for heavy vehicles. In: ASME-JSME-KSME 2011 Joint Fluids Engineering Conference. American Society of Mechanical Engineers, pp. 885–891.

Cheli, F., Belforte, P., Melzi, S., Sabbioni, E., Tomasini, G., 2006. Numericalexperimental approach for evaluating cross-wind aerodynamic effects on heavy vehicles. Vehicle System Dynamics 44 (sup1), 791–804.
URL http://dx.doi.org/10.1080/00423110600886689

Cooper, K. R., 04 2012. Wind tunnel and track tests of class 8 tractors pulling single and tandem trailers fitted with side skirts and boat-tails. SAE Int. J. Commer. Veh. 5, 1–17.
URL http://dx.doi.org/10.4271/2012-01-0104

Cooper, K. R., Leuschen, J., 11 2005. Model and full-scale wind tunnel tests of second-generation aerodynamic fuel saving devices for tractor-trailers. In: SAE Technical Paper. SAE International.
URL http://dx.doi.org/10.4271/2005-01-3512

Croll, R. H., Gutierrez, W. T., Hassan, B., Suazo, J. E., Riggins, A. J., 1996. Experimental investigation of the ground transportation systems (gts) project for heavy vehicle drag reduction. Tech. rep., SAE Technical Paper.

Gardell, L., 1980. Low drag truck cabs. Tech. rep., ScaniaDiv. Saab-Scania, Hausmitteilung.

Garry, K. P., Cooper, K. R., 1986. Comparison of quasi-static and dynamic wind tunnel measurements on simplified tractor-trailer models. Journal of Wind Engineering and Industrial Aerodynamics 22 (2), 185 – 194, special Issue 6th Colloquium on Industrial Aerodynamics Vehicle Aerodynamics.
URL http://www.sciencedirect.com/science/article/pii/0167610586900838

Gaylard, A. P., Duncan, B., apr 2011. Simulation of rear glass and body side vehicle soiling by road sprays. SAE International Journal of Passenger Cars - Mechanical Systems 4 (1), 184–196.
URL https://doi.org/10.4271/2011-01-0173

Heineck, J. T., Walker, S. M., Satran, D., 2004. The measurement of wake and gap flows of the generic conventional truck model (gcm) using three-component piv. In: The Aerodynamics of Heavy Vehicles: Trucks, Buses, and Trains. Springer, pp. 173–184.

Hucho, W.-H., 1987. Aerodynamics of road vehicles: from fluid mechanics to vehicle engineering. Elsevier.

Hyams, D. G., Sreenivas, K., Pankajakshan, R., Nichols, D. S., Briley, W. R., Whitfield, D. L., 2011. Computational simulation of model and full scale class 8 trucks with drag reduction devices. Computers & Fluids 41 (1), 27–40.

Landman, D., Wood, R., Seay, W., Bledsoe, J., 2010. Understanding practical limits to heavy truck drag reduction. SAE International Journal of Commercial Vehicles 2 (2), 183–190.

Leuschen, J., Cooper, K. R., 2006. Full-scale wind tunnel tests of production and prototype, second-generation aerodynamic drag-reducing devices for tractor-trailers. Tech. rep., SAE Technical Paper.

Maddox, S., Squires, K. D., Wurtzler, K. E., Forsythe, J. R., 2004. Detached-eddy simulation of the ground transportation system. In: The Aerodynamics of Heavy Vehicles: Trucks, Buses, and Trains. Springer, pp. 89–104.

McArthur, D., Burton, D., Thompson, M., Sheridan, J., 2016. On the wake of a simplified heavy vehicle. Journal of Fluids and Structures 0, 0.

McArthur, D. J., Burton, D., Thompson, M., Sheridan, J., 09 2013. Development of a wind tunnel test section for evaluation of heavy vehicle aerodynamic drag at a scale of 1:3. SAE Int. J. Commer. Veh. 6, 522–528.
URL http://dx.doi.org/10.4271/2013-01-2455

SAE, 2012. J1252_201207 sae wind tunnel test procedure for trucks and busses. Tech. rep., Society of Automotive Engineers.

Salari, K., Ortega, J., Castellucci, P., 2004. Computational prediction of aerodynamic forces for a simplified integrated tractor-trailer geometry. aiaa 2004-2253. In: 34th AIAA Fluid Dynamics Conference.

Storms, B. L., Satran, D. R., Heineck, J. T., Walker, S., 2004. A study of reynolds number effects and drag-reduction concepts on a generic tractor-trailer. AIAA paper 2251, 2004.

Storms, B. L., Satran, D. R., Heineck, J. T., Walker, S. M., 2006. A summary of the experimental results for a generic tractor-trailer in the ames research center 7-by 10-foot and 12-foot wind tunnels.

Tropea, C., Yarin, A. L., Foss, J. F., 2007. Springer handbook of experimental fluid mechanics. Vol. 1. Springer Science & Business Media.

Van Raemdonck, G. M. R., 2012. Design of Low Drag Bluff Road Vehicles. TU Delft, Delft University of Technology.

Weir, D. H., feb 1980. Truck splash and spray-some recent results. In: 1980 Automotive Engineering Congress and Exposition. SAE International.
URL https://doi.org/10.4271/800529